Polymer-encapsulated molecular doped epigraphene for quantum resistance metrology

OPEN ACCESS
IOP Publishing
Metrologia

Metrologia **56** (2019) 045004 (9pp)
https://doi.org/10.1088/1681-7575/ab2807

Polymer-encapsulated molecular doped epigraphene for quantum resistance metrology

Hans He[1], Samuel Lara-Avila[1,2], Kyung Ho Kim[1], Nick Fletcher[2], Sergiy Rozhko[2], Tobias Bergsten[3], Gunnar Eklund[3], Karin Cedergren[3], Rositsa Yakimova[4], Yung Woo Park[5,6], Alexander Tzalenchuk[2,7] and Sergey Kubatkin[1]

[1] Department of Microtechnology and Nanoscience, Chalmers University of Technology, S-41296 Göteborg, Sweden
[2] National Physical Laboratory, Hampton Road, Teddington TW11 0LW, United Kingdom
[3] RISE Research Institutes of Sweden, Box 857, S-50115 Borås, Sweden
[4] Department of Physics, Chemistry and Biology (IFM), Linköping University, S-58183 Linköping, Sweden
[5] Institute of Applied Physics, Seoul National University, Seoul 08826, Republic of Korea
[6] Department of Physics and Astronomy, University of Pennsylvania, Philadelphia, PA 19104, United States of America
[7] Royal Holloway, University of London, Egham TW20 0EX, United Kingdom

E-mail: hanshe@chalmers.se

Received 25 March 2019, revised 29 May 2019
Accepted for publication 10 June 2019
Published 28 June 2019

Abstract

One of the aspirations of quantum metrology is to deliver primary standards directly to end-users thereby significantly shortening the traceability chains and enabling more accurate products. Epitaxial graphene grown on silicon carbide (epigraphene) is known to be a viable candidate for a primary realisation of a quantum Hall resistance standard, surpassing conventional semiconductor two-dimensional electron gases, such as those based on GaAs, in terms of performance at higher temperatures and lower magnetic fields. The bottleneck in the realisation of a turn-key quantum resistance standard requiring minimum user intervention has so far been the need to fine-tune the carrier density in this material to fit the constraints imposed by a simple cryo-magnetic system. Previously demonstrated methods, such as via photo-chemistry or corona discharge, require application prior to every cool-down as well as specialist knowledge and equipment. To this end we perform metrological evaluation of epigraphene with carrier density tuned by a recently reported permanent molecular doping technique. Measurements at two National Metrology Institutes confirm accurate resistance quantisation below 5 $n\Omega\ \Omega^{-1}$. Furthermore, samples show no significant drift in carrier concentration and performance on multiple thermal cycles over three years. This development paves the way for dissemination of primary resistance standards based on epigraphene.

Keywords: molecular doping, graphene, measurement standards, quantum Hall effect

(Some figures may appear in colour only in the online journal)

1. Introduction

Epitaxial graphene on silicon carbide (epigraphene) can be grown as a high quality monocrystalline film on a wafer-scale, allowing for scalable production of electronic devices. The metrological viability of epigraphene as a quantum Hall resistance (QHR) standard was first shown experimentally in 2010 [1]. Epigraphene has since proven itself superior to the conventional two-dimensional electron gas (2DEG) systems based on GaAs/AlGaAs (henceforth simply GaAs) due to its unique electronic properties, which result in a robust quantum Hall effect (QHE) measurable at higher probing currents, higher temperatures and lower magnetic fields [2, 3]. The quantum Hall effect in epigraphene is so robust that the filling factor $\nu = 2$ plateau has been shown to extend over nearly 50 T [4]. Universality of the quantum Hall effect has been demonstrated to better than 0.1 n$\Omega\ \Omega^{-1}$ via comparison of resistance quantisation in epigraphene and GaAs [3, 5]. Finally, an epigraphene QHR standard was successfully operated at 4 K and 5 T in a small cryogen-free table-top system [2]. However, one major problem that remains is exerting control over the charge carrier density, which is necessary in order to achieve proper quantization and optimal operation for a chosen range of temperatures and magnetic fields. Under the above conditions, the empirically found [2] optimal carrier density yielding the maximum breakdown current is $(1.4 \pm 0.2) \times 10^{11}$ cm^{-2}, whereas metrologically useful currents $\gtrsim$10 μA can be achieved in 10 s μm wide devices in the approximate range of densities 0.5–2.5 $\times$ 10^{11} cm^{-2}. Due to the presence of an insulating interface layer (buffer layer) between the SiC substrate and graphene, epigraphene shows both high n-doping on the order of 10^{13} electrons per cm^2 and Fermi level pinning. These two factors in combination make tuning the carrier density to the useful range a challenge [6]. Previously tested methods such as photochemical gating [7, 8] and corona discharge [9] are suitable but lack the reliability and stability required for real-world applications. An interesting method of tuning the carrier density in epigraphene specifically for resistance metrology was demonstrated at NIST [10]. The method involves deposition of chromium tri-carbonyl on top of graphene followed by exposure to atmospheric air which relatively quickly reduces the carrier density to some usefully low level. However, according to [10] the carrier density continues to drift down by as much as 75% in one year and by then precision measurements suggest that the devices deviate from accurate quantisation by more than 10 n$\Omega\ \Omega^{-1}$. Ideally we would like to adjust the carrier density to the desired level once and for all during the epigraphene fabrication, as indeed is the situation for conventional GaAs devices.

A possible solution, involving polymer-assisted assembly of molecular dopants on the surface of epigraphene, has recently been proposed by the Chalmers group [11]. In this paper we demonstrate that this approach affords stable and controllable tuning of the charge carrier density in epigraphene while maintaining all of its major advantages for the realisation of a quantum resistance standard. We have explored long-term stability of molecularly doped epigraphene samples and compared the resistance quantisation to conventional GaAs resistance standards using cryogenic current-comparators (CCC) in two National Metrology Institutes (NMIs). We have also demonstrated stability upon repeated thermal cycles and operation of the standard in a dry table-top cryo-magnetic system.

2. Polymer-assisted molecular doping of epigraphene

2.1. Sample preparation

We have followed the procedure for sample fabrication and polymer-assisted assembly of molecular dopants as described in [11]. Here we summarise it briefly.

Epitaxial graphene was grown on the silicon face of an insulating 4H–SiC substrate using thermal decomposition of SiC at 2000 °C and in an 850 mbar argon atmosphere [12, 13]. The size of the SiC chips are 7 $\times$ 7 mm^2. Prior to microfabrication the highest quality of monolayer graphene chips, i.e. lowest amount of bilayer inclusions, are selected using transmission mode optical microscopy techniques [14]. The device fabrication was performed using standard electron beam lithography techniques to define electrical contacts and Hall bar devices. Excess graphene was removed using oxygen plasma etching and the resulting epigraphene Hall bars have typical dimensions of 30 $\times$ 150 μm^2 and are electrically contacted using 80 nm Au with 5 nm of Ti as an adhesion layer (see figure 1(a)).

The intrinsic n-doping of pristine epigraphene is on the order of 10^{13} electrons cm^{-2}. After microfabrication and exposure to ambient the carrier density tends to decrease, moving slightly towards neutrality [15]. However, the carrier density is usually too high to reliably observe fully developed quantum Hall effect below applied magnetic fields of 10 T, even at 2 K (see figure 2(b)). To achieve the desired carrier density, we apply polymer-assisted assembly of molecular dopants [11], which proceeds as follows: a 100 nm thick layer of the PMMA-F4TCNQ dopant blend is spin-coated onto a PMMA-protected sample, with a PMMA encapsulation layer on top. This sequence is then repeated to provide additional encapsulation and reduce drift of the carrier density (see figure 1(b)). The deposition of each polymer layer is followed by thermal annealing at 160 °C, above the PMMA glass transition temperature. The resulting carrier density can be fine-tuned through the total annealing time. For a concentration of 7% of F4TCNQ in PMMA by weight, and using the standardized annealing time, we have consistently observed a decrease in electron density by three orders of magnitude together with a tenfold increase of carrier mobility reaching 30 000–50 000 cm^2 V^{-1} s^{-1}. Several chemically doped epigraphene samples were prepared and measured in this study. Samples used to explore homogeneity of the doping were prepared with a deliberately low carrier density ~10^{10} cm^{-2} and these measurements are described in section 2.2. For the investigation of metrological viability samples were controllably tuned to ~1.5 $\times$ 10^{11} cm^{-2} in order to maximize the critical current in the desired operating regime for table-top systems

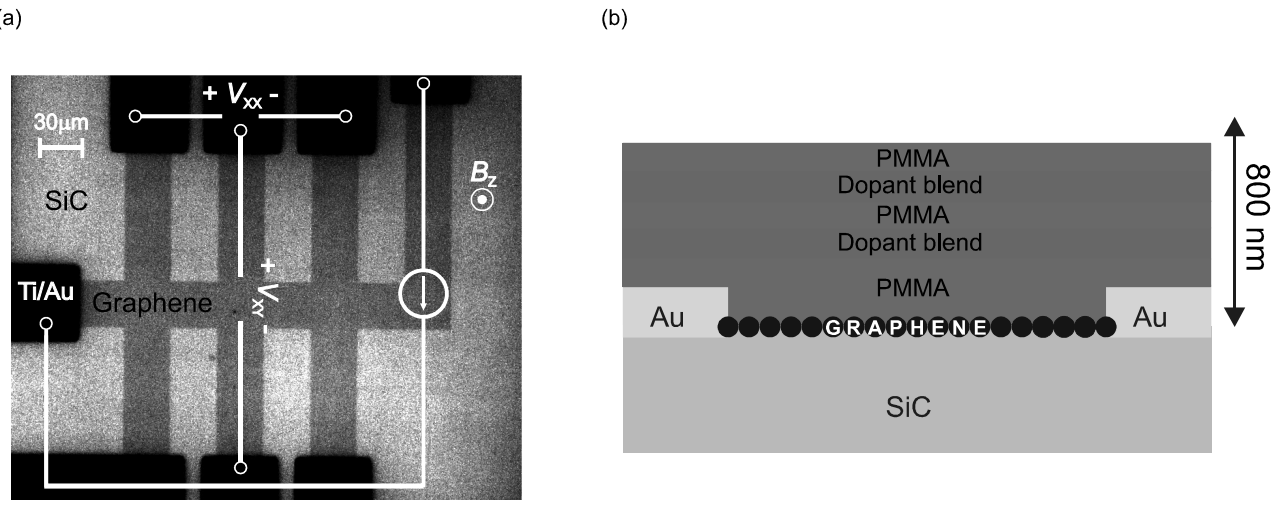

Figure 1. (a) Optical micrograph of a typical epigraphene Hall bar device taken in transmission mode. The overlay shows a schematic representation of the standard measurement setup for quantum Hall measurements with bias current direction, the direction of the perpendicular magnetic field, and connections for longitudinal voltage V_{XX} and Hall voltage V_{XY}. (b) Schematic representation of the chemical doping scheme consisting of an acceptor molecule encapsulated in organic polymers.

[2]. Figure 2(c) shows the long-time drift of the carrier density in two samples: one initially tuned to 5.4×10^{10} cm^{-2} and the other tuned to 1.63×10^{11} cm^{-2}. The electron density increased at an average relative rate 0.02% and 0.05% per day for the two samples respectively. The estimated lifetime of the two samples, that is the time they are expected to yield the breakdown current $\gtrsim$10 μA, is over 20 and 4 years respectively. Since the two samples differed not only in the initial carrier density but were also kept in different environments, dry nitrogen and vacuum, at room temperature between measurements, it is premature to speculate regarding the somewhat different, albeit by any measure very low, drift rate. The stability can potentially be improved even further by hermetic sealing or by storing the sample at low temperatures.

2.2. Large scale homogeneity

Understanding doping uniformity is important if the described fabrication method is to be used for reliable manufacturing of epigraphene QHR samples on a wafer scale. Figure 3 shows a comparison between molecular doping of microscopic and macroscopic Hall bars. Both devices have similar carrier densities, which in this case is low p-doping on the order $p \approx 10^{10}$ cm^{-2}, but drastically different surface areas (similarly n-doped samples show qualitatively similar behaviour). At such low carrier concentrations, where Fermi energy level is close to the Dirac point in graphene, the influence of the charge inhomogeneities on the measured resistance is more noticeable. The longitudinal and Hall resistance measurements were performed at 2 K using bias current 100 nA. For standard microscopic Hall bars with typical size 30×150 μm^2 we observe fully developed quantum Hall effect below 1 T, with a carrier density $p = 5.7 \times 10^9$ cm^{-2} and mobility $\mu = 52\,000$ cm^2 V^{-1} s^{-1}. For the macroscopic Hall bar of 5×5 mm^2 we also observe fully developed quantum Hall effect below 1 T, with carrier density $p = 9.1 \times 10^9$ cm^{-2} and mobility $\mu = 39\,000$ cm^2 V^{-1} s^{-1}. Note that we attribute the asymmetries in the low-field data to defects in graphene itself, such as bilayer inclusions and SiC steps, which can be avoided for smaller geometries [14] but not for macroscopic devices [16].

3. Metrological viability

For precision measurements we produced the following two samples: one sample G-RISE was measured at the Research Institutes of Sweden (RISE) in a liquid helium cryostat with an 11 T superconducting magnet and base temperature of 1.9 K, another sample G-NPL was tested at the National Physical Laboratory (NPL) in a small table-top mechanical refrigerator with the base temperature of 4 K and magnetic field 5 T [2]. The samples were manufactured at the same time but measured at different times over the span of almost two years. This time delay, and the different type of the cryogenic system could be considered as an additional test of reliability and stability of the molecularly gated graphene Hall devices. The electron concentration for G-RISE was initially tuned to around 1.3×10^{11} cm^{-2}, and 1.6×10^{11} cm^{-2} for G-NPL. The device geometries are identical to that of figure 1(a).

To evaluate the metrological viability of the epigraphene devices we have generally followed the technical guidelines for reliable DC measurements of the quantised Hall resistance initially developed for metal-oxide semiconductor field-effect transistors (MOSFETs) and GaAs devices [17]. Here we will consider the properties of the Hall devices which have the strongest effect on the precision of the Hall resistance measurements, such as the geometrical homogeneity of the 2D layer, the residual longitudinal resistance, the contact resistance, critical breakdown current, and finally analysis of the Quantum Hall resistance measurements using the CCC technique.

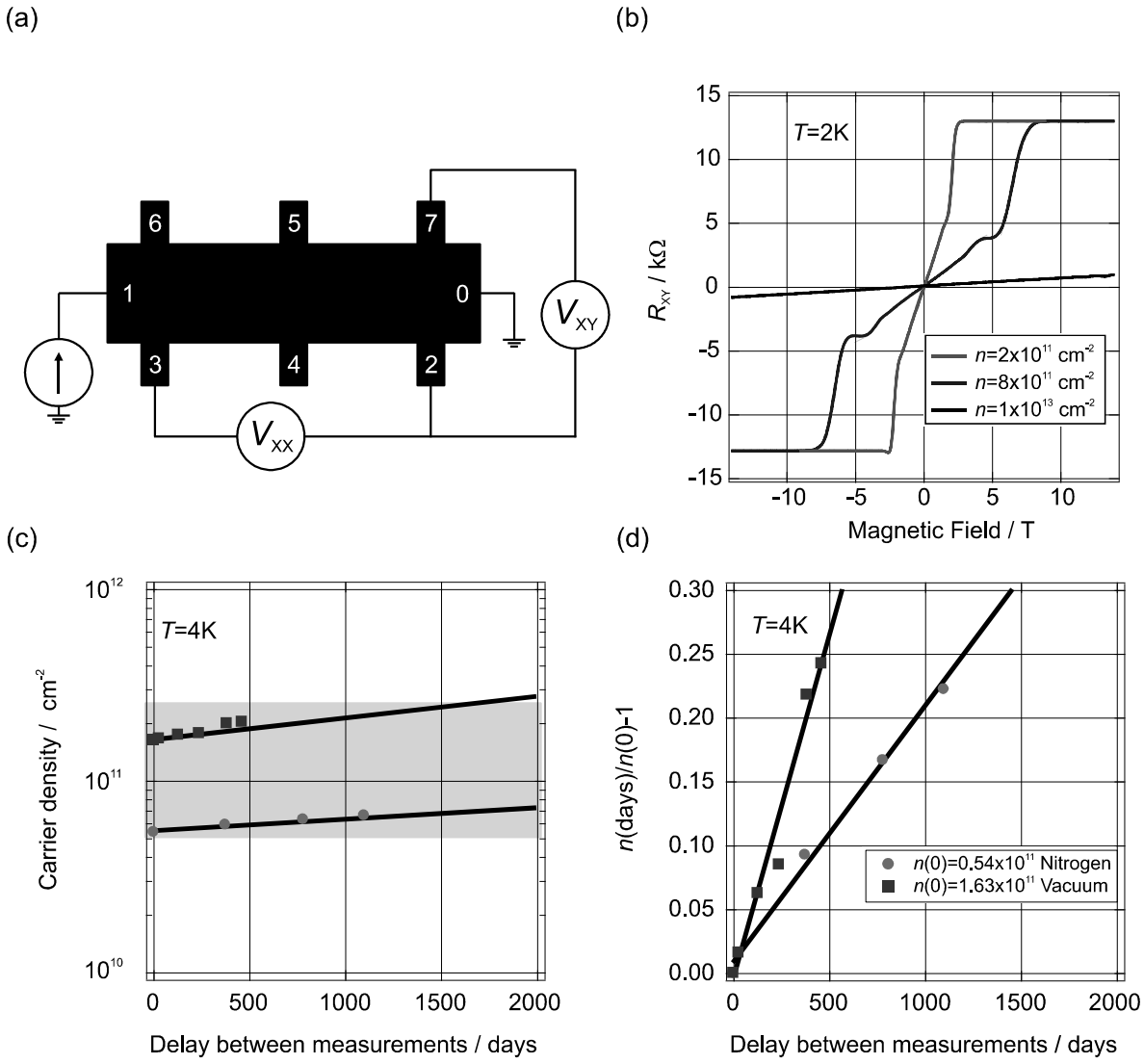

Figure 2. (a) Schematic sample layout and contact notations (b) measurements of Hall resistance R_{XY} performed at $T = 2\,\mathrm{K}$ with 100 nA bias, showing the different minimum magnetic field needed to reach the $\nu = 2$ plateau. The sample with the highest n-doping (black curve) corresponds to pristine epigraphene encapsulated by hexagonal boron nitride. The medium doped sample (blue curve), covered by polymer, shows the effect of partial compensation doping resulting mainly from polymer contaminants. The residual n-doping is typically above 10^{12} cm^{-2}. The sample with the lowest doping (red curve) was produced using chemical doping with an acceptor molecule. It has been controllably tuned to $n = 2 \times 10^{11}$ cm^{-2}. (c) Long term stability of carrier density measured in two samples described in the text. The green area indicates the limits of the carrier density set by the metrologically useful currents $\gtrsim 10\,\mu$A. The solid black lines are linear fits to the drift in carrier density. (d) The same data as (c) but plotted on the relative scale to highlight the linear drift.

3.1. Contact resistances measurements

All contact resistances were measured in the three-terminal configuration, in the magnetic field adjusted to the quantum Hall plateau (5 T). For illustration, the contact resistance for the sample G-NPL against DC current is presented in figure 4. Contact number is indicated on the graph. Note that pad #5 is not shown due to wire bond failure. All measured contact resistances were in the range of 0.1 to 1 Ω up to bias currents about 100 μA independent of current polarity, well below the recommended 10 Ω [18]. The sharp increase in resistance above 100 μA is due to the breakdown of the quantum Hall state. The same check was performed for sample G-RISE.

3.2. Critical current measurements

The critical breakdown current is the maximum non-dissipative current that the sample can sustain in the quantum Hall state. The onset of dissipation is seen in the abrupt increase of longitudinal resistance. Figure 5(a) shows R_{23} and R_{67} measured on both sides of the sample G-NPL against DC source-drain current of both polarities at $B = 5$ T and $T = 4\,\mathrm{K}$. The red points were measured on the 'low' potential side of the device and the black points—on the 'high' side. The apparent residual resistance $R_{23} \approx 1$ mΩ in the QHE regime disappeared when contact 1 instead of contact 0 was grounded [18]. It follows that the breakdown happens at $I_{SD} \approx 60$ μA with the accuracy of these measurements (at 10 nV level) for this

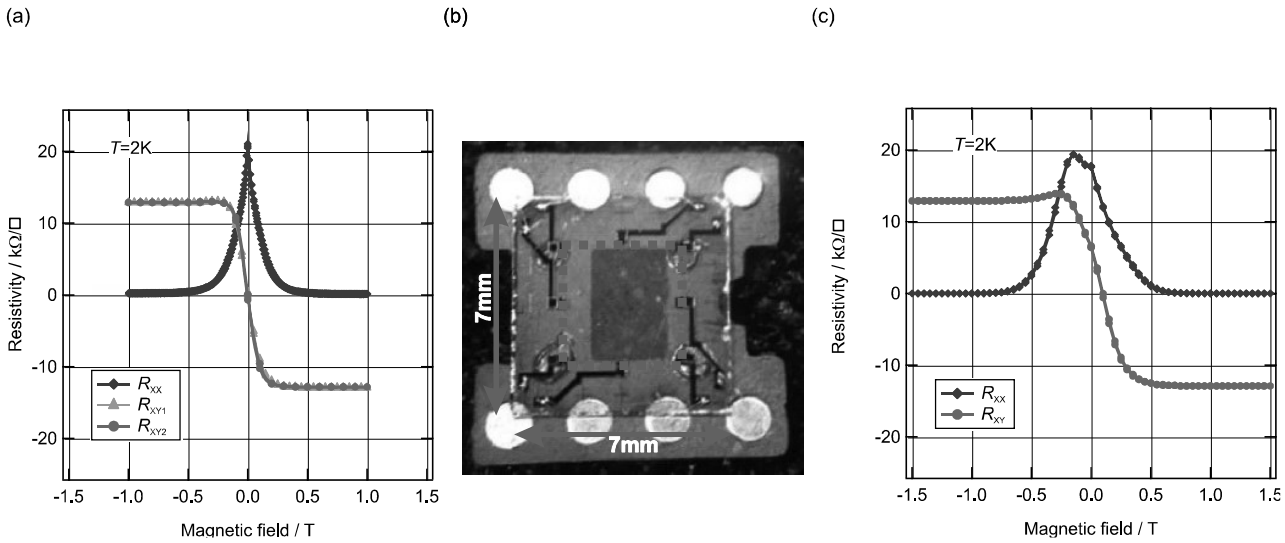

Figure 3. Chemical doping of epigraphene with low p-doping for both microscopic and macroscopic Hall bar geometries (a) quantum Hall measurements performed on 30 μm wide Hall bar, as seen in figure 1(a), displays fully quantized plateaus below 1 T. (b) Optical micrograph of a macroscopic Hall bar $5 \times 5\,\mathrm{mm}^2$. The red dotted square outlines the epigraphene region. Even at this scale the device is seemingly uniformly covered by the chemical dopant, as verified by (c) which shows quantization below 1 T. Adapted from [11]. CC BY 4.0.

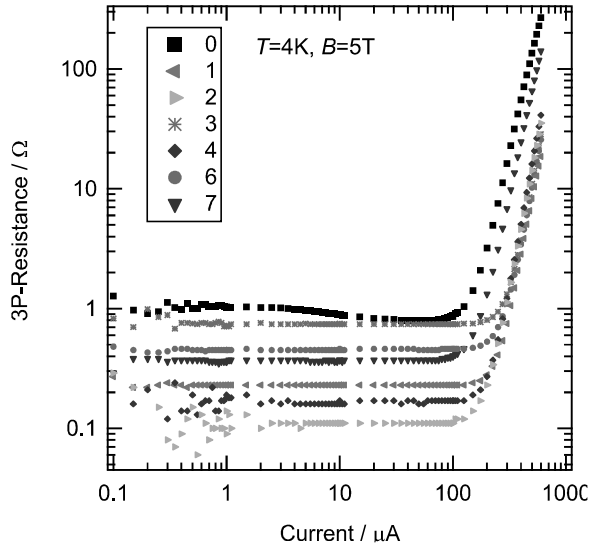

Figure 4. The contact resistance for sample G-NPL against DC current measured in three-probe configuration (3P). Numbers on the graph indicate the contact number, see figure 2(a).

particular sample. Figure 5(b) shows the critical currents for both measured samples, extracted as stated above, as a function of magnetic field. The difference in the critical currents is attributed to discrepancies between the two samples such carrier densities, charge homogeneity etc.

4. Precision measurements

The measurements described in the previous section (meeting the recommended guidelines for reliable QHR measurements) are in principle sufficient to demonstrate that the sample is fit for metrological use as a calibration reference. However, as the molecular gating represents a new fabrication technology, it is valuable to demonstrate the equivalence with an independent QHR realization in a proven GaAs sample. One possible cause of error that is not easily detected by the standard tests is a resistive leakage error in parallel with the quantized resistance, which might arise due to the surface dopant layer in our epigraphene device. A ratio comparison of the $\nu = 2$ and $\nu = 4$ plateaux in a GaAs sample can reveal this error, but this is not possible in a graphene device. In order to eliminate this or other possible undetected errors in the epigraphene sample we carried out a precision comparison to the GaAs reference using a cryogenic current comparator (CCC) based bridge.

The CCC bridges used for this comparison have been evaluated for absolute accurate measurements of the ratio 100 Ω:12.906 kΩ to a relative uncertainty of at least 10 nΩ Ω^{-1} [19]. The CCC device with its superconducting windings and shielding plus SQUID magnetic null detector provides the accurate dc current ratio required to achieve this. In this test, however, we are using the same instrument twice in almost identical conditions to make a substitution comparison between two QHR devices. Most of the uncertainty contributions and possible errors in the resistance measurement (for example ratio errors, imperfect detector linearity) cancel in this configuration, and the uncertainty budget for the comparison result is dramatically simplified. Ideally the type A (statistical) uncertainty of the measurements will be the limiting remaining component. The CCC bridge circuit is immune to most leakage paths (particularly leakage to screen) due to the use of an 'active Wagner' technique [19], but leakage directly across the QHR device is impossible to separate from the resistance being measured.

Similar measurements were carried out at both NPL and RISE and below we describe them in detail. Each NMI deliberately followed their own measurement protocol to maintain independent comparison.

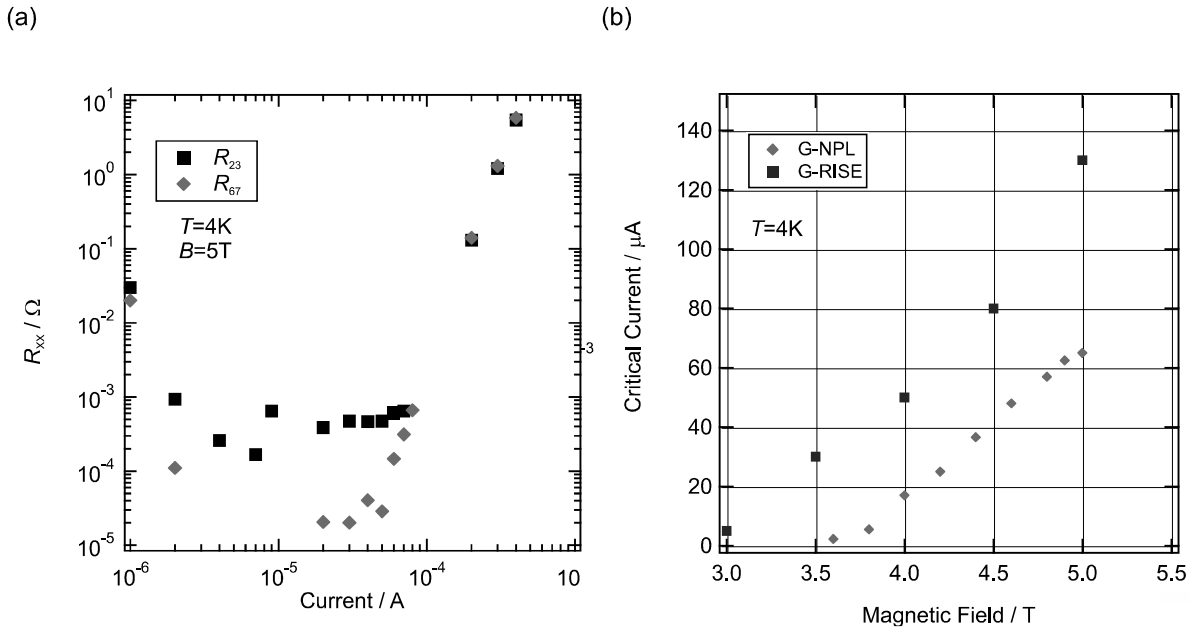

Figure 5. (a) Longitudinal resistance R_{XX} measured from the both sides of the sample using connections R_{23} and R_{67} for G-NPL plotted against DC source-drain current. (b) Critical current measured for sample G-NPL and G-RISE as a function of magnetic field.

4.1. CCC measurements on G-NPL

The comparison measurements at NPL use two separate cryomagnetic systems for epigraphene and GaAs. This allowed us to perform resistor calibration against one QHE device quickly followed by calibration against the other, and the first one again. The temperature and short term stability of the 100 Ω standard is then easily included in the type A evaluation via the 'A-B-A' measurement pattern and linear fit. As the QHR devices are in separate cryogenic systems, one effect that is independent and does not cancel is any leakage in the cryogenic wiring that appears in parallel with the QHR sample. The leakage in the GaAs system probe has previously been evaluated to contribute 10 pΩ Ω^{-1} relative uncertainty on a QHR measurement (i.e. to be $\geqslant 10^{15}$ Ω) [5]. The wiring in the table-top graphene system has been tested to $\geqslant 10^{14}$ Ω (0.1 nΩ Ω^{-1} relative uncertainty contribution).

The GaAs device used in the measurements at NPL was originally supplied by the Physikalisch-Technische Bundesanstalt (PTB), and has been in use for routine resistance traceability at NPL for over 20 years (and was one of the GaAs devices used in a previous comparison [5]). It has a carrier concentration of 4.6×10^{-11} cm^{-2} and mobility 400 000 cm^2 V^{-1} s^{-1}, and was operated on the $\nu = 2$ plateau at a temperature of <0.3 K and a magnetic field of 9.4 T in a conventional liquid helium cryostat. The comparison between this and the epigraphene device was performed via an intermediate 100 Ω conventional resistance standard, measured using the CCC bridge described in [19] with a 16:2065 turns ratio on the CCC. The current in the QHR device was 23 μA, giving nominally 3 mA or 1 mW power dissipation in the 100 Ω standard, which matches the regular calibration conditions. The epigraphene device was operated at 4.9 T and 4 K in the 'desktop' liquid free system described above.

Measurements were performed on several different 100 Ω standards, some of which were found to have short term instabilities that limited the overall uncertainty of the comparison. We give the results here of one comparison over 3 d (approximately 70 h of measurements) where the resistor showed a small linear drift. The resistor used was a Tinsley type wire wound Evanohm standard enclosed in a custom built thermostated enclosure with temperature stability of a few mK over the measurement period. The measurement sequence was graphene-GaAs-graphene in order to be able to cancel the effect of linear change of the 100 Ω standard. Figure 6(a) shows the results, plotted as the measured relative deviation of the unknown resistor from its nominal 100 Ω value, in μΩ Ω^{-1}. The CCC measurements consist of repeated forward and reverse current energization, with the bridge null detector reading analysed in forward-reverse-forward groups to eliminate offsets and drifts in the electronics. Each individual point on figure 6(a) is the result of this fitting for approximately 54 s of data, which is the shortest section that can be analysed in this way to give a calculated resistance value. To calculate the mean difference between the graphene and GaAs measurements we take a linear fit to the graphene data (two groups of blue points) and compare the value of this fit at the mean time of the GaAs data to the mean value of the GaAs data.

As the type A uncertainty contribution is effectively the total uncertainty for the comparison results, we need to take care that the usual expression for the standard uncertainty of the mean is a reliable estimate. Figure 6(b) presents the Allan deviation of the residuals to the linear fit for the three groups of data in figure 6(a). The Allan deviation in each case reduces as the square root of the measurement time (as expected for white noise with no time correlation) to below 1 nΩ Ω^{-1} (relative). This confirms the current reversal in the CCC measurements is successfully eliminating offset drifts and instabilities,

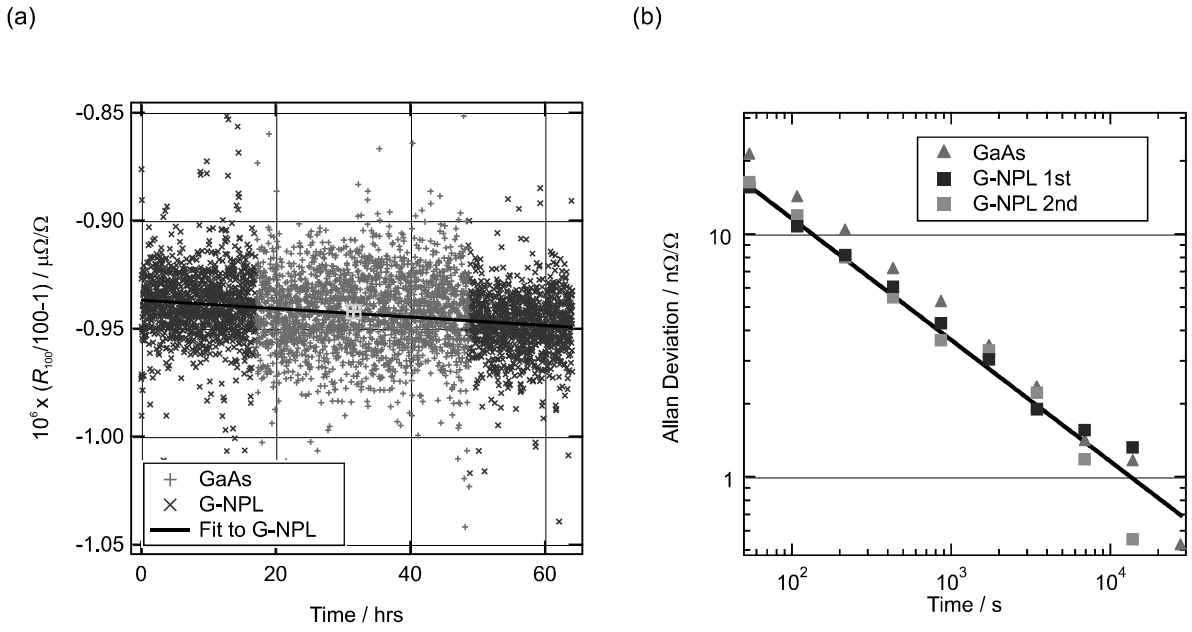

Figure 6. (a) Relative deviation of the 100 Ω standard resistor from its nominal 100 Ω value demonstrating linear drift. The linear fit to G-NPL data is shown by the solid black curve. The green square marks the mean value of GaAs at mean measurement time (b) Allan deviation of the residuals to the linear fit to data in (a). G-NPL 1st and 2nd denote the measurement using G-NPL before and after GaAs. The solid black line shows that the Allan deviation decreases with time τ as ~$1/\sqrt{\tau}$.

and that the linear drift model for the resistor is adequate. Although the reduction in uncertainty with increasing averaging time is as we would wish, the absolute level is larger than optimal. The ideal case measurement for our CCC bridge in this configuration should approach the Johnson noise limit for the resistors; for a cold QHR resistor and a room temperature 100 Ω this theoretical limit is around 2 nV $(\sqrt{\text{Hz}})^{-1}$ voltage noise, which translates to a relative uncertainty of 1 nΩ Ω^{-1} for a 100 s measurement at 1 mW measurement power. We observe a noise level approximately ten times worse than this, which is at least partly due to excess electromagnetic interference present in our laboratory. Despite this limitation, the extended measurement time with the automated bridge running continuously over 3 d does allow us to reach <1 nΩ Ω^{-1} final uncertainty, which is adequate to demonstrate the QHR device accuracy for all requirements in resistance traceability.

The final expanded uncertainty contains the root-sum-square of type A standard error of the mean for GaAs ($\sigma/\sqrt{N}$ here σ is standard deviation and N is number of samples), along with the uncertainty from the linear fit to G-NPL data. In summary, the difference in deviation from nominal of the 100 Ω resistor, Δ, as measured against the different QHR references is

$$\Delta_{\text{Gr–GaAs}} = 1.02 \pm 1.42\,\text{n}\Omega\,\Omega^{-1}(k = 2).$$

Epigraphene is shown to be in good agreement with standard GaAs.

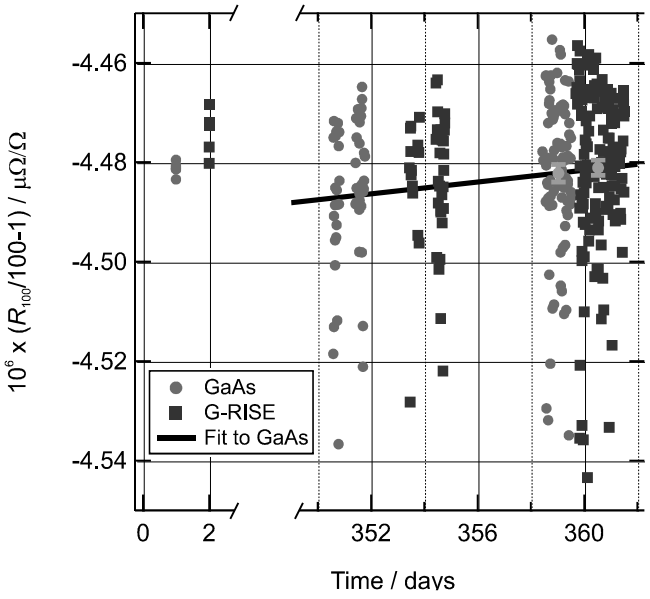

Figure 7. Comparison between sample G-RISE and a GaAs QHR device via a standard resistor with the nominal value of 100 Ω over the span of one year. The *y*-axis denotes the relative deviation from the nominal value of the 100 Ω resistor measured with the epigraphene and GaAs devices. The *x*-axis denotes the time in days from initial characterization. Each point is a 12 min long CCC measurement. The solid black line is a linear fit to the GaAs data taken from Day 350 and onwards. The green dots show the mean value at mean time for the last two GaAs and G-RISE measurement blocks. The bars represent the standard error of the means.

4.2. CCC measurements on sample G-RISE

RISE performed calibrations of a 100 Ω standard resistor against QHE devices, epigraphene and GaAs, sequentially in the same cryo-magnetic system. As mentioned, the advantage of this approach is that any leakage in the wiring of this measurement system will be cancelled out in the substitution measurement. The disadvantage is that swapping QHE devices over and repeating the measurements takes considerable time over which the comparison resistor may drift. The 100 Ω standard

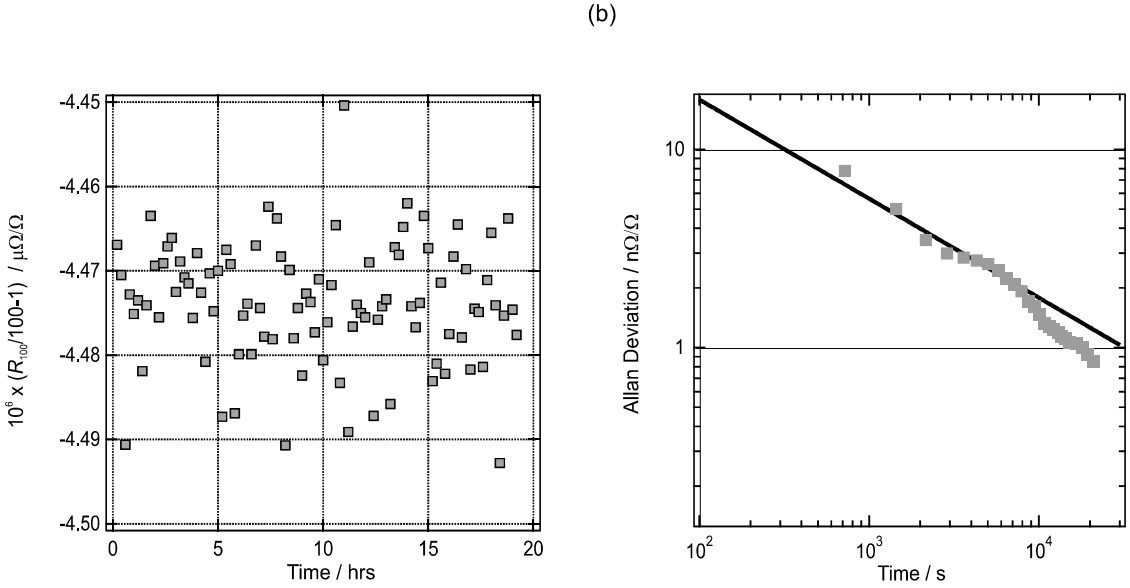

Figure 8. Extended CCC measurement of G-RISE compared to 100 Ω standard at 4.2 K, 8 T, and 23 μA bias. (a) Measured deviation from nominal value as a function of time, up to 20 h continuous measurements. Each data point corresponds to 12 min of measurement time. (b) Allan deviation calculated from the data in (a). The solid black line shows that the Allan deviation decreases with time ~$1/\sqrt{\tau}$.

resistor is a Tinsley AC/DC type 5685A which is stored in an oil bath kept at 25 °C, with a temperature stability of ~1 mK. Its short-term instability can be accounted for by introducing a significant type B uncertainty of 3 nΩ Ω^{-1}, or compensated for using 'A-B-A' type measurement as described above. The GaAs device used in these measurements at RISE also comes from PTB and has been in use for routine resistance traceability at RISE since 1999. The device has a carrier concentration of 5.2×10^{11} cm^{-2}, mobility 430 000 $cm^2\,V^{-1}\,s^{-1}$. It was operated on the $\nu = 2$ plateau at a temperature of 1.6–1.9 K and a magnetic field range between 9.65–9.95 T in a conventional liquid helium cryostat. The comparison was performed using a CCC bridge with a 32:4130 turns ratio on the CCC.

Figure 7 shows the two measurement campaigns of comparisons between sample G-RISE and GaAs performed over the span of one year. Each point takes 12 min to measure, which is the standard time for the CCC to finish one full, current reversed, measurement with the present setup.

From the initial set of measurements, up to Day 2, we can calculate that the difference between the mean relative deviations resulting from the G-RISE-100 Ω and GaAs-100 Ω CCC measurements as $\Delta_{\text{Gr–GaAs}} = 7.2 \pm 7.4$ nΩ Ω^{-1} ($k = 2$), including the root-sum-square of the type A standard error of the two means and an estimated type B error from instability of the 100 Ω standard. Figure 8(a) shows an extended measurement series where we continuously monitor the CCC measurement of G-RISE and 100 Ω standard over 20 h, with each point representing 12 min of measurement time. Figure 8(b) shows the Allan deviation which demonstrates how the precision improves over measurement time. The black dotted line shows that the Allan deviation predominately decreases with time ~$1/\sqrt{\tau}$ which indicates that uncorrelated white noise is the main source [20]. After six hours of continuous measurements we can reach <1 nΩ Ω^{-1} final uncertainty, which is a suitable level of device accuracy for all requirements in resistance traceability. This measurement shows agreement between G-RISE and GaAs within the expanded measurement error but can be improved by performing 'A-B-A' sequence to account for the short time linear drift component of the instability of the 100 Ω standard.

From day 350 and onwards an 'A-B-A-B' measurement was carried out. Since there is only one cryostat available, samples have to be exchanged in sequence, which takes a considerable time. However, the drift of the 100 Ω reference resistor appears to be linear inside these 10 d. Since the data blocks are more spread out in time compared to NPL the analysis is slightly different. A linear fit is performed on both blocks of GaAs data to estimate the drift in the resistor. We only look at the last two GaAs and G-RISE measurement blocks for two reasons. Firstly, they are closest in time and therefore, by comparing these two, the contribution of the uncertainty of the estimated linear drift is reduced. Secondly, they contain more than 71% of the measurement points which reduces the uncertainty of the mean value for these two points, compared to the others. We calculate the difference between the mean of GaAs points and mean of G-RISE points, with the linear drift of the 100 Ω standard subtracted. The final expanded uncertainty then contains the root-sum-square of type A standard error of the mean for both GaAs and G-RISE, along with the uncertainty of the estimated slope of the GaAs data acquired from fitting. In summary, the difference in deviation from nominal of the 100 Ω resistor, Δ, as measured against the different QHR references is

$$\Delta_{\text{Gr–GaAs}} = 0.19 \pm 4.81\ \text{n}\Omega\,\Omega^{-1} (k = 2).$$

Epigraphene is again shown to be in good agreement with GaAs standard. It is also shown to retain its performance in CCC measurements for at least one year.

5. Conclusions

The new molecular doping scheme enables uniform precision control of the carrier density in epitaxial graphene on SiC, which remains stable over at least several years despite numerous thermal cycles. Independent measurements in two NMIs confirmed that the molecularly gated epigraphene devices are suitable for realization of the SI resistance unit at the level of uncertainty required in any metrology laboratory.

Acknowledgment

This work was jointly supported by the Swedish-Korean Basic Research Cooperative Program of the NRF (No. NRF-2017R1A2A1A18070721), the Swedish Foundation for Strategic Research (SSF) (No. IS14-0053, GMT14-0077, and RMA15-0024), Swedish Research Council (VR), VINNOVA, Knut and Alice Wallenberg Foundation, Chalmers Area of Advance NANO, the UK Department of Business, Energy and Industrial Strategy (BEIS), and the European Union's Horizon 2020 research and innovation programme under Grant Agreement GrapheneCore2 No 785219.

ORCID iDs

Nick Fletcher https://orcid.org/0000-0002-9653-1580
Yung Woo Park https://orcid.org/0000-0003-2046-8025
Sergey Kubatkin https://orcid.org/0000-0001-8551-9247

References

[1] Tzalenchuk A, Lara-Avila S, Kalaboukhov A, Paolillo S, Syväjärvi M, Yakimova R, Kazakova O, Janssen T J B M, Fal'ko V and Kubatkin S 2010 Towards a quantum resistance standard based on epitaxial graphene *Nat. Nanotechnol.* **5** 186–9

[2] Janssen T J B M, Rozhko S, Antonov I, Tzalenchuk A, Williams J M, Melhem Z, He H, Lara-Avila S, Kubatkin S and Yakimova R 2015 Operation of graphene quantum Hall resistance standard in a cryogen-free table-top system *2D Mater.* **2** 035015

[3] Ribeiro-Palau R *et al* 2015 Quantum Hall resistance standard in graphene devices under relaxed experimental conditions *Nat. Nanotechnol.* **10** 1–18

[4] Alexander-Webber J A *et al* 2016 Giant quantum Hall plateaus generated by charge transfer in epitaxial graphene *Sci. Rep.* **6** 30296

[5] Janssen T J B M, Fletcher N E, Goebel R, Williams J M, Tzalenchuk A, Yakimova R, Kubatkin S, Lara-Avila S, Falko V I and Yakimova R 2011 Graphene, universality of the quantum Hall effect and redefinition of the SI system *New J. Phys.* **9** 93026

[6] Kopylov S, Tzalenchuk A, Kubatkin S and Fal'Ko V I 2010 Charge transfer between epitaxial graphene and silicon carbide *Appl. Phys. Lett.* **97** 112109

[7] Lara-Avila S, Moth-Poulsen K, Yakimova R, Bjaßrnholm T, Fal'Ko V, Tzalenchuk A and Kubatkin S 2011 Non-volatile photochemical gating of an epitaxial graphene/polymer heterostructure *Adv. Mater.* **23** 878–82

[8] Tzalenchuk A *et al* 2011 Engineering and metrology of epitaxial graphene *Solid State Commun.* **151** 1094–9

[9] Lartsev A, Yager T, Bergsten T, Tzalenchuk A, Janssen T J B M, Yakimova R, Lara-Avila S and Kubatkin S 2014 Tuning carrier density across Dirac point in epitaxial graphene on SiC by corona discharge *Appl. Phys. Lett.* **105** 063106

[10] Rigosi A F *et al* 2018 Gateless and reversible Carrier density tunability in epitaxial graphene devices functionalized with chromium tricarbonyl *Carbon* **142** 468–74

[11] He H *et al* 2018 Uniform doping of graphene close to the Dirac point by polymer-assisted assembly of molecular dopants *Nat. Commun.* **9** 3–9

[12] Emtsev K V *et al* 2009 Towards wafer-size graphene layers by atmospheric pressure graphitization of silicon carbide *Nat. Mater.* **8** 203–7

[13] Virojanadara C, Syväjarvi M, Yakimova R, Johansson L, Zakharov a and Balasubramanian T 2008 Homogeneous large-area graphene layer growth on 6H-SiC(0 0 0 1) *Phys. Rev.* B **78** 245403

[14] Yager T *et al* 2013 Express optical analysis of epitaxial graphene on SiC: impact of morphology on quantum transport *Nano Lett.* **13** 4217–23

[15] Panchal V, Giusca C E, Lartsev A, Martin N A, Cassidy N, Myers-Ward R L, Gaskill D K and Kazakova O 2016 Atmospheric doping effects in epitaxial graphene: correlation of local and global electrical studies *2D Mater.* **3** 015006

[16] Yager T, Lartsev A, Yakimova R, Lara-Avila S and Kubatkin S 2015 Wafer-scale homogeneity of transport properties in epitaxial graphene on SiC *Carbon* **87** 409–14

[17] Delahaye F 1989 Technical guidelines for reliable measurements of the quantized hall resistance *Metrologia* **26** 63–8

[18] Delahaye F and Jeckelmann B 2003 Revised technical guidelines for reliable dc measurements of the quantized Hall resistance *Metrologia* **40** 217–23

[19] Williams J M, Janssen T J B M, Rietveld G and Houtzager E 2010 An automated cryogenic current comparator resistance ratio bridge for routine resistance measurements *Metrologia* **47** 167–74

[20] Allan D W 1987 Should the classical variance be used as a basic measure in standards metrology? *IEEE Trans. Instrum. Meas.* **IM–36** 646–54